ADVANCED MATERIALS
www.advmat.de

Engineering Spin-Orbit Interactions in Silicon Qubits at the Atomic-Scale

*Yu-Ling Hsueh, Daniel Keith, Yousun Chung, Samuel K. Gorman, Ludwik Kranz, Serajum Monir, Zachary Kembrey, Joris G. Keizer, Rajib Rahman, and Michelle Y. Simmons**

Spin-orbit interactions arise whenever the bulk inversion symmetry and/or structural inversion symmetry of a crystal is broken providing a bridge between a qubit's spin and orbital degree of freedom. While strong interactions can facilitate fast qubit operations by all-electrical control, they also provide a mechanism to couple charge noise thereby limiting qubit lifetimes. Previously believed to be negligible in bulk silicon, recent silicon nano-electronic devices have shown larger than bulk spin-orbit coupling strengths from Dresselhaus and Rashba couplings. Here, it is shown that with precision placement of phosphorus atoms in silicon along the [110] direction (without inversion symmetry) or [111] direction (with inversion symmetry), a wide range of Dresselhaus and Rashba coupling strength can be achieved from zero to 1113 × 10^{-13}eV-cm. It is shown that with precision placement of phosphorus atoms, the local symmetry (C_{2v}, D_{2d}, and D_{3d}) can be changed to engineer spin-orbit interactions. Since spin-orbit interactions affect both qubit operation and lifetimes, understanding their impact is essential for quantum processor design.

1. Introduction

Spin-orbit interactions in solid state devices are central to many applications in spintronics[1–4] ranging from spin field-effect-transistors[5,6] to magnetic random-access memories.[7–9] Controlling spin-orbit interactions in quantum processors is also essential, since they are responsible for all-electrical control of spins using electric dipole spin resonance (EDSR)[10–16] and spin-orbit mediated decoherence processes.[17–30] This is particularly the case for semiconductor spin qubits.[31–34] Spin-orbit interactions also form one of the key ingredients for semiconductor-based topological qubits.[35–37] Fundamentally, spin-orbit interactions are linked to the inherent symmetry found in solids. Two of the most well-known forms of spin-orbit coupling, are Rashba and Dresselhaus coupling, which arise when either the structural or bulk inversion symmetry is broken in a material, respectively.[38,39] The former typically arises at surfaces and interfaces in a solid, while the latter occurs in materials with distinct anion and cation sites such as gallium-arsenide (GaAs) and indium-arsenide (InAs). In contrast, a silicon (Si) crystal inherently possesses inversion symmetry, such that Desselhaus spin-orbit interactions are absent in the bulk material. However, in addition to structural and bulk inversion asymmetries, we also have to consider interface inversion asymmetries, which can arise from asymmetric bonding of atoms at heterostructure interfaces, which also result in Dresselhaus and/or Rashba spin-orbit interactions.[40–43] Therefore when considering quantum confinement of qubits in semiconductor nanostructures, the local symmetry resulting from the microscopic details of the confinement potential in the immediate crystalline environment plays a significant role in determining the spin-orbit interactions present in the system.

The form and strength of spin-orbit interactions are often extracted from measuring electron spin splitting/g-factor and/or spin-relaxation (T_1) processes. For electrons bound to single phosphorus (P) donors in bulk Si, spin-orbit coupling was found to be very weak ($g_l - g_t = 0.001$, where g_l and g_t are the Si conduction band valley longitudinal and transverse effective g factor, respectively. This gives the spin-orbit term

Y.-L. Hsueh, D. Keith, Y. Chung, S. K. Gorman, L. Kranz, S. Monir, J. G. Keizer, R. Rahman, M. Y. Simmons
Silicon Quantum Computing Pty Ltd.
Level 2, Newton Building, UNSW Sydney, Kensington, NSW 2052, Australia
E-mail: michelle.simmons@unsw.edu.au
Y.-L. Hsueh, S. Monir, Z. Kembrey, R. Rahman
School of Physics
University of New South Wales
Sydney, NSW 2052, Australia
D. Keith, Y. Chung, S. K. Gorman, L. Kranz, J. G. Keizer, M. Y. Simmons
Centre of Excellence for Quantum Computation and Communication Technology
School of Physics
University of New South Wales
Sydney, NSW 2052, Australia

The ORCID identification number(s) for the author(s) of this article can be found under https://doi.org/10.1002/adma.202312736

DOI: 10.1002/adma.202312736

Table 1. Comparison of the spin-orbit strength in a 2P molecule from this work to that of a single donor, a Si-MOS-based quantum dot and a SiGe quantum dot system.

Qubit	Dresselhaus strength, α_D [eV-cm]	Rashba strength, α_R [eV-cm]	Combined strength, $\alpha = \alpha_D + \alpha_R$ [eV-cm]	H_{EB} strength [e m T^{-1}]
2P donor molecule [this work]	556×10^{-13}	556×10^{-13}	1113×10^{-13}	4.71×10^{-14}
Single donor[24]	–	–	–	5.86×10^{-14}
Si-MOS quantum dot[46]	178×10^{-13}	15×10^{-13}	193×10^{-13}	–
SiGe quantum dot[42]	10×10^{-13}	1×10^{-13}	11×10^{-13}	–

H_{SO} ≈0.06 μeV at $B = 1$ T).[44,45] However in quantum confined nano-structures, in both SiGe and Si-metal-oxide-semiconductor (Si-MOS) quantum dots, anisotropic electron spin-splittings,[42,46] and spin-relaxation[18,20–22,47] have been shown to be dominated by Dresselhaus and Rashba spin-orbit interactions with values of $H_{SO} \approx 0.1 - 2$ μeV. Here, the presence of vertical electric fields in gate defined quantum dots has led to large Rashba spin-orbit strengths in Si-MOS dots (15×10^{-13} eV-cm[46]). The microscopic interface inversion asymmetry present in both SiGe dots and Si-MOS dots has also led to a large Dresselhaus spin-orbit coupling strength ($10 - 178 \times 10^{-13}$ eV-cm[42,46]), see **Table 1**.

With the advent of atomic precision scanning tunneling microscope (STM) lithography,[48,49] individual P atoms can now be selectively placed in Si along different lattice directions within the crystal. With high confidence in the reproducible precision manufacturing afforded[49,50] we now have a unique, and hitherto unexplored mechanism to engineer the local symmetry, and thereby spin-orbit interactions in Si. In particular, we show how placing two donors along different crystalline directions creates different local symmetries with spin-orbit interactions ranging from C_{2v} (without inversion symmetry) along the [110] direction to D_{2d} (without inversion symmetry) along the [100] direction and D_{3d} (with inversion symmetry) along the [111] direction. This variation cannot be obtained by a single donor in Si, where the symmetry is always T_d (without inversion symmetry).

2. Spin-Orbit Interactions in Two Donor Atoms

Figure 1 shows different atomistic symmetries of two phosphorus (2P) donors in the crystal lattice and the corresponding spin-orbit interactions. If we place the two donor atoms along the [110] crystalline axis, the system demonstrates C_{2v} symmetry,[51] where it is invariant under 180° rotation about the [001] axis, and reflections about the (110) and ($\bar{1}$10) planes (see Figure 1a). In this case, there is no inversion symmetry in the system and both Dresselhaus and Rashba spin-orbit interactions can occur[41] (see Figure 1d). If the two donors are separated along the [100] crystalline axis, the symmetry is D_{2d}[51] (see Figure 1b). This group contains symmetry operations for each of the following operations: 180° rotations about the x, y, and z-axis; reflections about the (110) and ($\bar{1}$10) planes; and the 90° rotation about the [001] axis followed by a reflection in the horizontal plane (the S_4 operator). Here, compared to the C_{2v} group, Rashba spin-orbit interaction is no longer invariant under the S_4 operator in this D_{2d} symmetry group, allowing only the Dresselhaus spin-orbit (see Figure 1e). If the two donors are however separated along the [111] crystalline axis, with a separation distance ($N \pm 0.25$, $N \pm 0.25$, $N \pm 0.25)a_0$, where N is an integer and $a_0 = 0.543$ nm is the Si lattice constant, then the system belongs to the D_{3d} symmetry group[51] (see Figure 1c). The system is invariant under operations such as C_3 (120° rotations about the [111] axis), σ_d (reflections about the ($\bar{1}$10), (01$\bar{1}$), and (10$\bar{1}$) planes) and inversion (about the midpoint of the two donors, see Figure 1f). Here since the system possesses an inversion center, both Dresselhaus and Rashba spin-orbit couplings are no longer allowed. We can therefore in principle engineer spin-qubits with different spin-orbit interactions by placing the two donors at specific atomic locations in the Si crystal with the STM technique.[48]

3. $1/T_1$ Anisotropy: Theory Versus Experiment

A key way to investigate the nature of spin-orbit interactions is to obtain $1/T_1$ data as a function of the external magnetic field orientation.[52,53] Spin-relaxation processes in donor qubits have been shown to arise mainly from phonons or charge noise both of which require a spin-orbit coupling mechanism.[24] The coupling mechanism can arise from either Dresselhaus, Rashba, electromagnetic[24] and/or hyperfine coupling to the nuclear spin.[54] Each mechanism is anisotropic with magnetic field orientation but with a different form, and magnitude of dependence.

For a single donor device with the external electric field pointing along the [010] direction ($\phi = 90°$), a clear anisotropy was observed in the value of $1/T_1$ at $B = 3.5$ T as we change the magnetic field orientation. This was explained by phonon induced spin-relaxation[24] where the longest T_1 recorded was 1.25 s when the external magnetic field was pointed in the same direction [010]. These results could be explained by the presence of an electromagnetic spin-orbit interaction (H_{EB}) mediated phonon relaxation mechanism that becomes zero when both the external electric and magnetic fields are aligned. The presence of H_{EB} in these single donor systems arises from the inversion symmetry breaking from the presence of the P donor atom.

To see the impact of symmetry arguments on the spin-orbit interactions present in 2P molecule qubits, we used atomistic tight-binding calculations (see Methods). Specifically we modeled the charge noise induced $1/T_1$ anisotropy (see Section S1, Supporting Information for how we obtained $1/T_1$ from atomically resolved electronic states including spin-orbit interactions) for 2P donor atoms separated along the [110], [100], and [111] directions, as shown in **Figure 2a,b**. To model the charge noise known to be present in our devices[55] we consider the dominating noise source - two-level fluctuators (TLFs) present at the native oxide surface. We then benchmarked our model against experimental noise measurements, where we obtained $S_{E0} = 3.80$

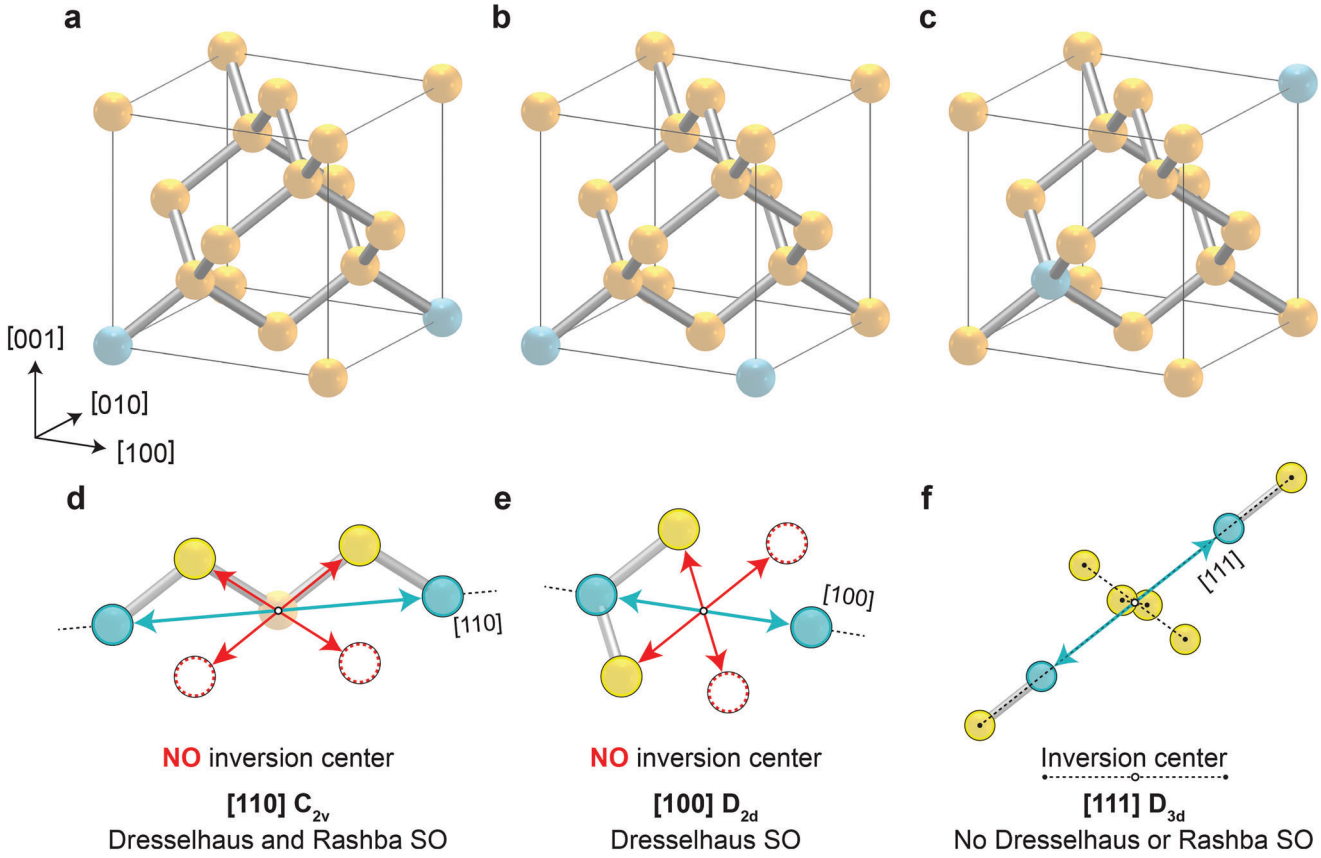

Figure 1. Engineering spin-orbit terms at the microscopic level from local symmetries. In a system with 2P donors (cyan spheres represent the P atoms and yellow spheres represent the Si atoms), the symmetry group depends on the orientation of the inter-donor axis with respect to the crystal lattice. a,d) When the 2P donors are placed along the [110] crystalline axis, the system possesses C_{2v} symmetry where inversion symmetry is broken as indicated by the red arrows representing the inversion operation transforming the Si atoms (yellow dots) to the red-dotted circles where the corresponding Si atoms are absent. This then results in both Dresselhaus and Rashba spin-orbit interactions present in the system. b,e) When the 2P donors are placed along the [100] crystalline axis, the system possesses D_{2d} symmetry. Here again inversion symmetry is broken resulting in Dresselhaus spin-orbit interaction present in the system. However Rashba spin-orbit interaction is not allowed. c,f) In contrast, when the 2P donors are placed along the [111] crystalline axis with the separation shown in the figure, the system possesses D_{3d} symmetry with inversion symmetry (all the atoms transform to each other under the inversion operation). Here both Dresselhaus and Rashba spin-orbit interactions are no longer allowed.

$\times 10^{-7}(\mathrm{MV/m})^2$ at 1 Hz (see Sections S2 and S3, Supporting Information for the model details and charge noise measurements, respectively). For a [100]-separated 2P molecule, possessing D_{2d} symmetry, the Dresselhaus spin-orbit interaction has the form $-k_y\sigma_y + k_z\sigma_z$, resulting in an effective magnetic field along $[0\bar{1}1]$, since $\langle k_y\rangle = \langle k_z\rangle$ for the [100]-separated donors. Therefore, when the external magnetic field (B) is perpendicular to the effective magnetic field produced by the spin-orbit interaction, such as B||[100], the spin-mixing is largest that results in maximum $1/T_1$. When the two donors are however separated along [111] by either $0.75a_0$ or $1.75a_0$, the system possesses D_{3d} symmetry. Here, the presence of inversion symmetry results in no Dresselhaus and Rashba spin-orbit interactions. This is confirmed by our atomistic calculations where we see zero spin-orbit mediated charge noise relaxation. Therefore, to achieve the longest T_1 for any external magnetic field direction, the two P atoms in a 2P molecular qubit should be placed along the [111] direction with an inversion center and hence no spin-orbit coupling. For a [110]-separated 2P molecule, which possesses C_{2v} symmetry, the Dresselhaus spin-orbit interaction has the form $-k_x\sigma_x + k_y\sigma_y$ and the Rashba spin-orbit interaction has the form $k_x\sigma_y - k_y\sigma_x$. This results in an effective magnetic field B^{eff} produced by either the Dresselhaus term or the Rashba term pointing along the $[\bar{1}10]$ crystalline axis, since $\langle k_x\rangle = \langle k_y\rangle$. If the external magnetic field (B) or the spin polarization axis is perpendicular to the effective magnetic field B^{eff} produced by the spin-orbit interaction, such as B||[110], the electron spin has maximum spin-orbit mixing that results in maximum $1/T_1$. However, when both the external magnetic field and the effective magnetic field point in the same direction (along $[\bar{1}10]$) then there is no spin-orbit mixing and therefore minimal relaxation so $1/T_1$ is the smallest. From these simulations, we see that the orientation of the donors in the crystal significantly affects the spin-orbit coupling observed.

We now experimentally investigate spin-orbit interactions in a device with 2P atoms patterned in Si using STM lithography along the [110] direction[50] to see if we observe the predicted behavior from Figure 2a. Along this orientation the donor atoms have C_{2v} symmetry in which both Dresselhaus and Rashba spin-orbit interactions will be present. We measure the T_1 times in this donor molecule as a function of the external magnetic field

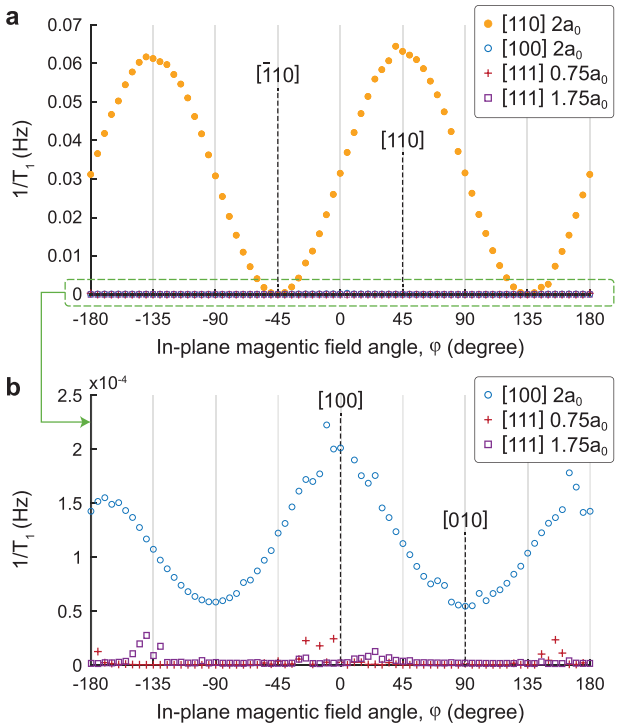

Figure 2. $1/T_1$ magnetic field anisotropy for 2P molecular qubits oriented along the [110], [100], or [111] crystalline directions. a) Atomistic calculations of Dresselhaus and Rashba spin-orbit mediated charge noise relaxation anisotropy in a 2P molecule separated by $2a_0$ along [110] or [100], $0.75a_0$ along [111] or $1.75a_0$ along [111]. Note the different distances are dictated by the atomic locations in the Si crystal. b) A zoomed-in plot of $1/T_1$ for the 2P atoms separated by either $0.75a_0$ or $1.75a_0$ along [111] confirming that with D_{3d} the presence of inversion symmetry results in both Dresselhaus and Rashba spin-orbit interactions being prohibited in contrast to when the 2P atoms are separated by $2a_0$ along [100] in D_{2d} symmetry where Dresselhaus spin-orbit interaction is still present with a variation of $1/T_1$ with in-plane magnetic field angle.

angle with respect to the Si crystal axis at $B = 1.5$ T. **Figure 3a** shows the device layout and relevant crystalline directions. The measured data is shown by the black vertical bars including errors in Figure 3b–d. Importantly, to achieve these results we use a newly developed ramped readout technique that allows us to access the low magnetic field regime ($B < 1.5$ T) whilst maintaining high readout fidelity above 99%.[56]. We observed the longest $T_1 \approx 40$ s when the external magnetic field aligned along the effective spin-orbit field B ∥ [1̄10] for $\theta = 90°$ and $\phi = 135°$, and shortest $T_1 \approx 11$ s when B ⊥ [1̄10], B∥[001] ($\theta = 0°$ in Figure 3b) and the plane with $\phi = 45°$ (shown in Figure 3c), confirming our predictions.

We observe that the spin-orbit mechanisms follow the same anisotropy as the theoretical calculations but a different magnitude. We can understand this if we consider other spin relaxation mechanisms in our system. In addition to both the Dresselhaus and Rashba spin-orbit mediated charge noise relaxation mechanisms, we must also consider H_{EB} mediated charge noise, and hyperfine mediated phonon relaxation (see Section S4, Supporting Information for a comprehensive theoretical description of all the relaxation mechanisms present in our devices). We characterize the strength of each mechanism in Section S5 (Supporting Information). The results from a single least-error fit to all the $1/T_1$ experimental data is shown as the blue lines in Figure 3b–d. Here the Dresselhaus/Rashba spin-orbit mediated charge noise relaxation is shown as the solid blue lines, the H_{EB} mediated charge noise relaxation as the dashed blue lines, the hyperfine mediated phonon relaxation as the dotted blue lines, and the total relaxation rate obtained from summing up all three relaxation mechanisms shown as the dash-dotted blue lines. We find that the Dresselhaus and Rashba spin-orbit mediated charge noise $1/T_1$ anisotropy and magnitude (the solid blue lines in Figure 3b–d) are captured quantitatively by the atomistic calculations from Figure 2a when, we consider the 2P donors being separated along [110] by $2a_0$, see the yellow dots in Figure 3b–d, for not only the in-plane but also the out-of-plane magnetic field rotations. The blue surface in Figure 3e represents the T_1 values (of all theory mechanisms combined) at $|\mathbf{B}| = 1.5$ T in 3D space for all possible magnetic field orientations. The longest $T_1 = 40$ s confirmed experimentally is when B ∥ [1̄10].

Other relaxation mechanisms, such as the spin-orbit mediated phonon relaxation and hyperfine mediated charge noise relaxation are not dominating at $B = 1.5$ T (see Section S4, Supporting Information) but can have a small contribution to the T_1 anisotropy curve. In addition, we note that two sources of spin–spin interactions can occur in these multi-spin systems. The first is the anisotropic hyperfine interaction between the electron and the two phosphorus nuclear spins and the second is the dipolar coupling between the nuclear spins. Both, in principle, can result in additional couplings that could affect spin-relaxation in these devices. The strength of the anisotropic hyperfine term in a 2P system is however 2–3 orders of magnitude smaller than the contact hyperfine[57] and therefore negligible. Whilst the flip-flopping of the nuclear spins would not affect the spin relaxation times,[58] it could however add to the magnetic noise from the surrounding ^{29}Si that would contribute to the T_2 decoherence process.

4. $1/T_1$ B Dependence: Theory Versus Experiment

Having presented a detailed explanation of the observed T_1 anisotropy at $B = 1.5$ T in Figure 3, we can now model and measure the total value of $1/T_1$ at different magnetic field strengths. Here, we fix the magnetic field direction to the [110] crystal axis with $\theta = 90°$ and $\phi = 45°$. The black error bars shown in **Figure 4** represent the measured data. We compare this with the different magnetic field dependencies for each spin-relaxation mechanism (discussed in detail in Section S6, Supporting Information). The dashed blue line represents the sum of Dresselhaus/Rashba and H_{EB} spin-orbit mediated charge noise induced spin relaxation, which has a linear B dependency. Here, the combined magnitude is taken from the results of T_1 anisotropy data in Figure 3. The dashed-dotted blue line is the hyperfine mediated phonon relaxation mechanism, which follows a B^3 dependency, with the magnitude extracted from the T_1 anisotropy fit. The dotted blue line represents the B^5 spin-orbit mediated phonon relaxation. The magnitude of the spin-orbit mediated phonon relaxation is estimated from Ref. [50], which measured T_1 in the high B field regime ($B > 1.5$ T) for the same 2P device as in this work. Summing up all the different relaxation mechanisms gives the solid blue line, in close agreement with the experimental data (black error bars) without any additional fitting involved.

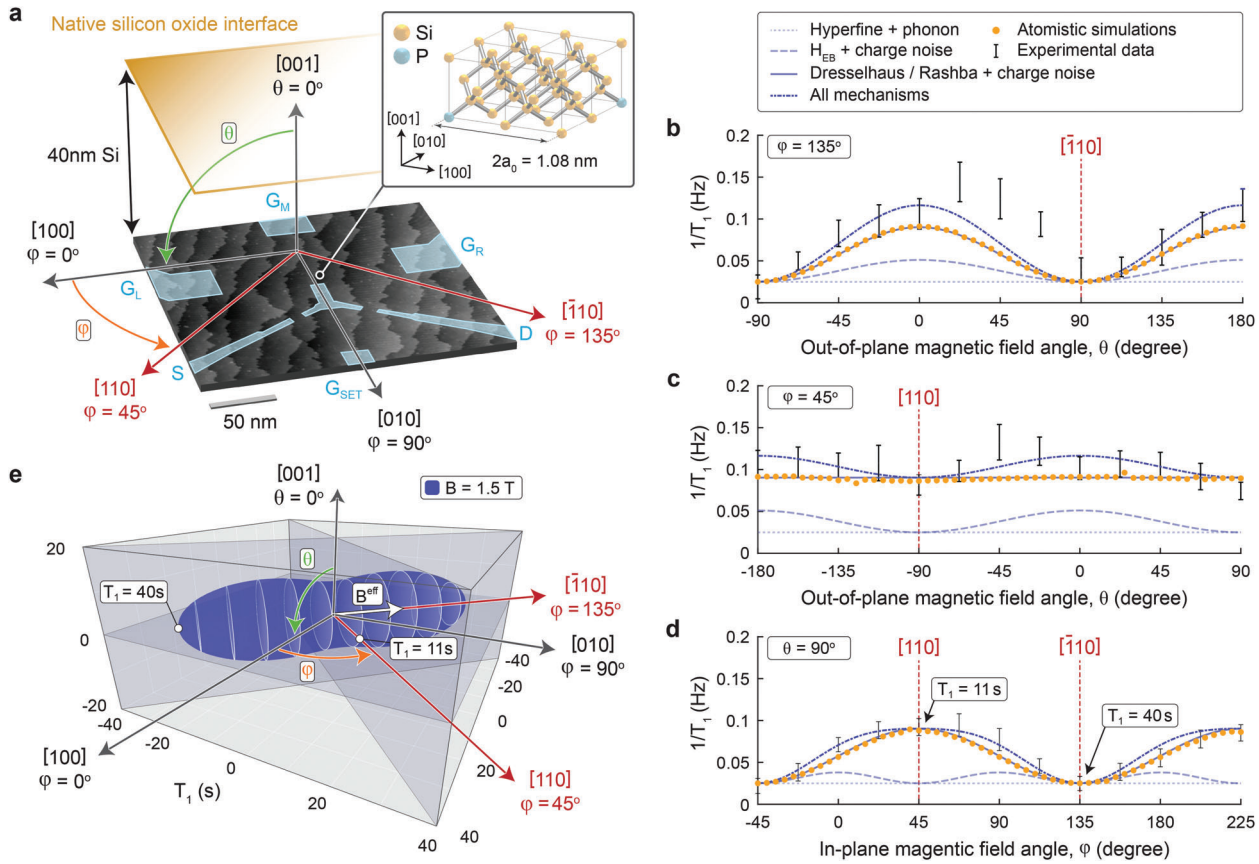

Figure 3. Spin-orbit interactions in a 2P molecular qubit from $1/T_1$ magnetic field anisotropy. a) An STM image of the device showing the locations of the surrounding in-plane P doped gates (G_L, G_R, G_M, and G_{SET} - the blue shaded regions); along with the source (S) and drain (D) and the 2P donors located at the white circle near the center of the device. If we consider the donor location within the crystal (top right) we see they are oriented along the [110] direction and separated by 1.5 nm. Around the STM image we highlight the orientation of the chip with respect to the crystalline Si axes and the location of the SiO_2 interface 40nm above. Here, the device is encapsulated in Si and sits 40 nm below this native oxide surface, which is the main source of 1/f charge noise causing decoherence through spin-orbit interactions. To probe the spin-orbit interactions we can rotate the orientation of magnetic field along different Si crystal axes using a vector magnet (θ out-of-plane and ϕ in-plane) and measure the resulting T_1 time at $B = 1.5$ T. b) Out-of-plane magnetic field rotation at a fixed angle of $\phi = 135°$. c) Out-of-plane magnetic field rotation at a fixed angle of $\phi = 45°$. d) In-plane rotation at a fixed angle of $\theta = 90°$. e) Resulting T_1 values at $|B_{ext}| = 1.5$ T for all mechanisms combined at all magnetic field orientations. The longest T_1 (or smallest $1/T_1$) of 40 s is observed when the external magnetic field is aligned in the same direction as the effective magnetic field B^{eff} pointing along the [1̄10] direction ($\theta = 90°$, $\phi = 135°$) and perpendicular to the inter-donor axis ([110]). T_1 becomes short ($T_1 \approx 11$ s) when the external magnetic field is perpendicular to B^{eff} (along [001], [110] and the whole $\phi = 45°$ plane), thereby mixing the spins.

For this donor orientation, [110], and magnetic field angle $\phi = 45°$ we know that the effective spin-orbit mixing is largest resulting in the shortest T_1 times of 11 s at $B_{\parallel} = 1.5$ T, see Figure 3d. Being able to reduce the magnitude of the external magnetic field to $B_{\parallel} = 0.75$ T whilst performing spin readout using our recently published ramped readout technique,[56] we show we can increase this T_1 time to 43 s. From our theory we show that it is in principle possible to achieve even longer T_1 times of ≈ 320 s at $B_{\perp} = 0.75$ T (see Figure 4) by choosing $\phi = 135°$ or B ∥ [1̄10], where no effective spin-orbit mixing exists. At this point, we are only left with hyperfine mediated phonon relaxation (see the dashed vertical line [1̄10] and $T_1 = 40$ s in Figure 3d) that would result in the largest values of $T_1 \approx 320$ s. We did not measure this T_1 time due to the prohibitively long measurement time (see Methods).

Table 2 shows a comparison of the longest T_1 times to date in different semiconductor spin qubits. Interestingly, the longest T_1 time of 57 s reported to date has been achieved in a GaAs quantum dot despite the presence of Dresselhaus spin-orbit (with strength $\approx 140 \times 10^{-13}$ eV-cm[53]) in this system. To achieve this the authors used low magnetic fields $B = 0.6 - 0.7$ T aligned along the [1̄10] magnetic field orientation to suppress the spin-orbit mediated phonon relaxation. In their results only hyperfine mediated phonon relaxation dominated. Therefore, despite having a strongly spin-orbit coupled system they were able to mitigate spin relaxation by suppressing Dresselhaus coupling with magnetic field angle.

With the ultimate precision placement of donors in all x, y, and z orientations recently achieved[63] we show that if we align the donors along the [111] direction, with complete inversion symmetry we can eliminate both Dresselhaus and Rashba spin-orbit mechanisms. Importantly, by placing P atoms in this orientation, we show that it is possible to achieve T_1 of hundreds of seconds at $B = 0.75$ T for all magnetic field angles. Our results therefore highlight the benefits of atomic precision engineering of the local symmetry

Table 2. Comparison of the longest T_1 times reported in literature for different semiconductor qubits.[59]

System [Ref.]	T_1	$\|B_{ext}\|$	B_{ext} orientation	Dominating spin relaxation mechanism
GaAs/AlGaAs quantum dot[53]	57 s	0.6-0.7 T	[$\bar{1}$10]	Hyperfine mediated phonon relaxation
2P donor molecule [this work]	40 s	1.5 T	[$\bar{1}$10]	Hyperfine mediated phonon relaxation
2P donor molecule [this work]	43 s	0.75 T	[110]	Spin-orbit mediated charge noise relaxation
Single donor[60]	9.8 s	1 T	[110]	Evanescent wave Johnson noise
Single donor[24]	9.3 s	1.25 T	[110]	Spin-orbit mediated charge noise relaxation
Si-MOS quantum dot[61]	9 s	1 T	≈102° to [100]	Spin-orbit mediated phonon or charge noise relaxation
SiGe quantum dot[62]	5 s	0.4 T	[110]	Spin-orbit mediated charge noise relaxation

and thereby spin-orbit interactions for high-fidelity qubit operations.

5. Estimating the Magnitude of Spin-Orbit Coupling Strengths

We extract the magnitude of the spin-orbit interaction in our 2P molecular qubit from charge noise induced $1/T_1$ anisotropy results. Here, the electric-field noise amplitude, $S_{E0} = 3.80 \times 10^{-7}$(MV/m)^2 at 1 Hz as obtained previously. The combined Dresselhaus and Rashba spin-orbit strength ($\alpha = \alpha_D + \alpha_R = 1113 \times 10^{-13}$ eV-cm) is extracted from the solid blue line in Figure 3b, corresponding to the Dresselhaus/Rashba spin-orbit interactions mediated charge noise relaxation (see Section S7, Supporting Information). Independently, we confirmed the spin-orbit strength directly from atomistic calculations, and obtained $\alpha = 1094 \times 10^{-13}$ eV-cm (see Section S8, Supporting Information). From projecting the spin-orbit perturbed spin states to the unperturbed (no spin-orbit) states (see Section S9, Supporting Information), we show that $\alpha_D = \alpha_R = 556 \times 10^{-13}$ eV-cm, i.e., where both Dresselhaus and Rashba spin-orbit interactions have equal strengths. This is not surprising since they both arise from the microscopic symmetry breaking of the 2P atoms separated along [110]. Table 1 shows a comparison of the spin-orbit strengths measured and/or modeled in different Si nanostructures. Importantly, the combined spin-orbit strength of the 2P molecule $\alpha = 1113 \times 10^{-13}$ eV-cm is around six times larger than the combined spin-orbit interactions available in a Si-MOS-based quantum dot where $\alpha = 193 \times 10^{-13}$ eV-cm,[46] and two-orders of magnitude larger than the combined spin-orbit interactions in a SiGe quantum dot where $\alpha = 11 \times 10^{-13}$ eV-cm.[42]

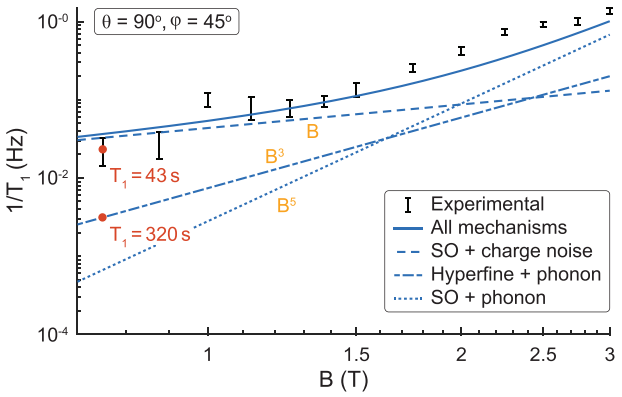

Figure 4. Magnetic field dependence of spin-relaxation for a 2P molecule oriented along [110]. The measured data (black error bars) can be quantitatively described by a combination of spin-relaxation mechanisms: spin-orbit mediated phonon relaxation (B^5), hyperfine mediated phonon relaxation (B^3) and spin-orbit mediated charge noise relaxation (B). The longest T_1 time at this magnetic field orientation B||[110] is 43 s which is achieved when $B = 0.75$ T. It is possible to achieve longer T_1 of 320 s if B || [$\bar{1}$10] instead of B||[110] .

It is also possible to extract the H_{EB} spin-orbit interaction constant $C = C_l - C_t = 4.71 \times 10^{-14}$ e m T^{-1} (see Equation (S3), Supporting Information) from the dashed blue line in Figure 3b, which corresponds to the H_{EB} spin-orbit interaction mediated charge noise relaxation mechanism (see Section S10, Supporting Information). The H_{EB} strength $C = 4.71 \times 10^{-14}$ e m T^{-1} is very similar to that measured for single donors $C = 5.86 \times 10^{-14}$ e m T^{-1}.[24] These results confirm that the 2P molecule Bohr radius ≈1–2 nm[19] in this device has a similar confinement radius compared to a single 1P donor ≈2 nm. Importantly this highlights the much stronger confinement potential in atom based systems compared to Si-MOS-based quantum dots with dot radii ≈10 nm and SiGe quantum dots with dot radii ≈30–100 nm. It is this strong confinement potential that leads to such strong spin-orbit couplings - achieved here by placing two P atoms in Si along [110] and binding one electron. In doing so, we show we can increase the spin-orbit coupling from ≈ 0.06 μeV[44,45] to 33.9 μeV (see Section S7, Supporting Information).

6. Conclusion

In conclusion, we have demonstrated the importance of the microscopic nature of quantum confinement on the local symmetry and hence spin-orbit interactions in Si qubits. By placing two P atoms ≈ 1.5 nm apart along the [110] crystalline direction with the C_{2v} symmetry group using STM lithography, we show we can engineer a large spin-orbit coupling strength of 1113×10^{-13} eV-cm. By then aligning the magnetic field orientation perpendicular to the inter-donor axis (B⊥[110]), we can minimize this spin-orbit mediated charge noise relaxation process to extend the T_1 times to 40 s at $B = 1.5$ T. We further show that operating the qubits at even lower magnetic fields, where Dresselhaus and Rashba spin-orbit are minimized will result in longer T_1 times up to 320 s at $B = 0.75$ T. Our results also indicate that by placing the donors along the [111] crystallographic direction with a D_{3d} symmetry group that contains an inherent inversion symmetry, we can minimize Dresselhaus and Rashba spin-orbit coupling completely. For this crystalline symmetry only hyperfine mediated phonon

relaxation exists, which results in long T_1 times for all magnetic field angles. Our detailed theoretical and experimental investigation of local microscopic symmetries in the qubit environment provides essential information for engineering spin-orbit interactions in semiconductor quantum processors as we scale.

7. Methods

Experiment: The T_1 measurement was performed by loading a random electron spin on the 2P qubit and reading out the spin after a certain wait time.[64] The extremely long relaxation times measured in the device mean that the measurement time required to extract a single T_1 value was also long. Each measured T_1 value consisted of a repetitive measurement of the device for approximately 13 h. Therefore, each Figure 3a,b,c took a measurement time of approximately 170 h or 7 d and a total of 21 d to complete the whole measurement along all three rotations. This measurement time was orders of magnitude longer than most experiments in quantum dots[59] and was only possible due to the very stable, low charge noise donor-based devices.[65] Despite this low charge noise it was interesting to note that the long measurement time ultimately was the cause of the large error bars (see Figure 3a–c).

Atomistic Calculations: A large scale atomistic tight binding method was used with spin resolved $sp^3d^5s^*$ atomic orbitals with nearest neighbor interactions.[66] Each donor was modeled as a positive charge center creating a Coulomb potential screened by the dielectric constant of Si and a cut-off potential U_0 at the donor site representing the central-cell correction.[67] The two donor atoms were placed at the center of a 20 nm^3 Si box (consist of 0.4 millions of Si atoms) such that the donor wavefunctions were not affected by the boundaries of the box. The donor wavefunctions from this model were shown to give accurate hyperfine constants.[68,69] The intrinsic Si spin-orbit interaction was included by introducing a matrix element coupling the atomic p-orbitals with opposite spins of each Si atom.[70] Dresselhaus, Rashba, and other spin-orbit interactions fall out automatically as the system/Hamiltonian was constructed with the required symmetry, atom by atom.[42]

Supporting Information

Supporting Information is available from the Wiley Online Library or from the author.

Acknowledgements

The authors would like to thank valuable discussions with Prof. Leonid Golub about the symmetry operations and the corresponding spin-orbit interaction in Si quantum well, Prof. Roland Winkler about the spin-orbit interactions in single donors and Prof. Xuedong Hu about the relaxation mechanisms in Si quantum dots. This research was conducted by Silicon Quantum Computing Pty Ltd and the Australian Research Council Centre of Excellence for Quantum Computation and Communication Technology (CE170100012). M.Y.S. acknowledges an Australian Research Council Laureate Fellowship and is CEO of Silicon Quantum Computing. The research was undertaken with the assistance of resources and services from the National Computational Infrastructure (NCI) under NCMAS 2020, 2021 and 2022 allocation, supported by the Australian Government, and of the computational cluster Katana supported by Research Technology Services at UNSW Sydney.

Open access publishing facilitated by University of New South Wales, as part of the Wiley - University of New South Wales agreement via the Council of Australian University Librarians.

Author Contributions

D.K., Y.C., and S.K.G. performed the measurements. D.K., Y.C., S.K.G., L.K., and J.K. analyzed the data. Y.H., S.M., Z.K., and R.R. developed the theory. M.Y.S. and R.R. supervised the project. Y.H., S.K.G., L.K., J.K., R.R. and M.Y.S. wrote the paper with input from all authors.

Conflict of Interest

M.Y.S. is a director of the company Silicon Quantum Computing Pty Ltd.

Data Availability Statement

The data that support the findings of this study are available from the corresponding author upon reasonable request.

Keywords

dresselhaus, inversion symmetry, rashba, scanning tunnelling microscope, semiconductor qubit, spin-orbit interaction, spin-relaxation

Received: November 26, 2023
Revised: February 25, 2024
Published online: April 9, 2024

[1] I. Žutić, J. Fabian, S. D. Sarma, *Rev. Mod. Phys.* **2004**, *76*, 323.
[2] A. Manchon, H. C. Koo, J. Nitta, S. M. Frolov, R. A. Duine, *Nat. Mater.* **2015**, *14*, 871.
[3] A. Avsar, H. Ochoa, F. Guinea, B. Özyilmaz, B. Van Wees, I. J. Vera-Marun, *Rev. Mod. Phys.* **2020**, *92*, 021003.
[4] A. Hirohata, K. Yamada, Y. Nakatani, I.-L. Prejbeanu, B. Diény, P. Pirro, B. Hillebrands, *J. Magn. Magn. Mater.* **2020**, *509*, 166711.
[5] S. Datta, B. Das, *Appl. Phys. Lett.* **1990**, *56*, 665.
[6] P. Chuang, S.-C. Ho, L. W. Smith, F. Sfigakis, M. Pepper, C.-H. Chen, J.-C. Fan, J. Griffiths, I. Farrer, H. E. Beere, G. A. C. Jones, D. A. Ritchie, T.-M. Chen, *Nat. Nanotechnol.* **2015**, *10*, 35.
[7] D. D. Awschalom, M. E. Flatté, *Nat. Phys.* **2007**, *3*, 153.
[8] B. Dieny, I. L. Prejbeanu, K. Garello, P. Gambardella, P. Freitas, R. Lehndorff, W. Raberg, U. Ebels, S. O. Demokritov, J. Akerman, A. Deac, P. Pirro, C. Adelmann, A. Anane, A. V. Chumak, A. Hirohata, S. Mangin, S. O. Valenzuela, M. C. Onbasli, M. d'Aquino, G. Prenat, G. Finocchio, L. Lopez-Diaz, R. Chantrell, O. Chubykalo-Fesenko, P. Bortolotti, *Nat. Electron.* **2020**, *3*, 446.
[9] Q. Shao, P. Li, L. Liu, H. Yang, S. Fukami, A. Razavi, H. Wu, K. Wang, F. Freimuth, Y. Mokrousov, M. D. Stiles, S. Emori, A. Hoffmann, J. Åkerman, K. Roy, J.-P. Wang, S.-H. Yang, K. Garello, W. Zhang, *IEEE Trans. Magn.* **2021**, *57*, 1.
[10] S. Nadj-Perge, S. Frolov, E. Bakkers, L. P. Kouwenhoven, *Nature* **2010**, *468*, 1084.
[11] B. Venitucci, L. Bourdet, D. Pouzada, Y.-M. Niquet, *Phys. Rev. B* **2018**, *98*, 155319.
[12] N. Hendrickx, D. Franke, A. Sammak, G. Scappucci, M. Veldhorst, *Nature* **2020**, *577*, 487.
[13] F. N. Froning, L. C. Camenzind, O. A. van der Molen, A. Li, E. P. Bakkers, D. M. Zumbühl, F. R. Braakman, *Nat. Nanotechnol.* **2021**, *16*, 308.
[14] K. Wang, G. Xu, F. Gao, H. Liu, R.-L. Ma, X. Zhang, Z. Wang, G. Cao, T. Wang, J.-J. Zhang, D. Culcer, X. Hu, H.-W. Jiang, H.-O. Li, G.-C. Guo, G.-P. Guo, *Nat. Commun.* **2022**, *13*, 1.
[15] E. N. Osika, S. Kocsis, Y.-L. Hsueh, S. Monir, C. Chua, H. Lam, B. Voisin, M. Y. Simmons, S. Rogge, R. Rahman, *Phys. Rev. Appl.* **2022**, *17*, 054007.
[16] W. Gilbert, T. Tanttu, W. H. Lim, M. Feng, J. Y. Huang, J. D. Cifuentes, S. Serrano, P. Y. Mai, R. C. Leon, C. C. Escott, K. M. Itoh, N. V.

Abrosimov, H.-J. Pohl, M. L. W. Thewalt, F. E. Hudson, A. Morello, A. Laucht, C. H. Yang, A. Saraiva, A. S. Dzurak, *Nat. Nanotechnol.* **2023**, *18*, 131.
[17] D. Culcer, X. Hu, S. Das Sarma, *Appl. Phys. Lett.* **2009**, *95*, 073102.
[18] P. Huang, X. Hu, *Phys. Rev. B* **2013**, *88*, 075301.
[19] Y.-L. Hsueh, H. Büch, Y. Tan, Y. Wang, L. C. L. Hollenberg, G. Klimeck, M. Y. Simmons, R. Rahman, *Phys. Rev. Lett.* **2014**, *113*, 246406.
[20] P. Huang, X. Hu, *Phys. Rev. B* **2014**, *90*, 235315.
[21] C. Tahan, R. Joynt, *Phys. Rev. B* **2014**, *89*, 075302.
[22] P. Huang, X. Hu, *Phys. Rev. B* **2014**, *89*, 195302.
[23] A. Bermeister, D. Keith, D. Culcer, *Appl. Phys. Lett.* **2014**, *105*, 192102.
[24] B. Weber, Y.-L. Hsueh, T. F. Watson, R. Li, A. R. Hamilton, L. C. L. Hollenberg, R. Rahman, M. Y. Simmons, *npj Quantum Inf.* **2018**, *4*, 61.
[25] J. Yoneda, K. Takeda, T. Otsuka, T. Nakajima, M. R. Delbecq, G. Allison, T. Honda, T. Kodera, S. Oda, Y. Hoshi, N. Usami, K. M. Itoh, S. Tarucha, *Nat. Nanotechnol.* **2018**, *13*, 102.
[26] T. Kobayashi, J. Salfi, C. Chua, J. Van Der Heijden, M. G. House, D. Culcer, W. D. Hutchison, B. C. Johnson, J. C. McCallum, H. Riemann, N. V. Abrosimov, P. Becker, H.-J. Pohl, M. Y. Simmons, S. Rogge, *Nat. Mater.* **2021**, *20*, 38.
[27] S. Bosco, B. Hetényi, D. Loss, *PRX Quantum* **2021**, *2*, 010348.
[28] Z. Wang, E. Marcellina, A. Hamilton, J. H. Cullen, S. Rogge, J. Salfi, D. Culcer, *npj Quantum Inf.* **2021**, *7*, 1.
[29] Y. Choi, R. Joynt, *npj Quantum Inf.* **2022**, *8*, 1.
[30] O. Malkoc, P. Stano, D. Loss, *Phys. Rev. Lett.* **2022**, *129*, 247701.
[31] F. A. Zwanenburg, A. S. Dzurak, A. Morello, M. Y. Simmons, L. C. Hollenberg, G. Klimeck, S. Rogge, S. N. Coppersmith, M. A. Eriksson, *Rev. Mod. Phys.* **2013**, *85*, 961.
[32] A. Chatterjee, P. Stevenson, S. De Franceschi, A. Morello, N. P. de Leon, F. Kuemmeth, *Nat. Rev. Phys.* **2021**, *3*, 157.
[33] N. P. De Leon, K. M. Itoh, D. Kim, K. K. Mehta, T. E. Northup, H. Paik, B. Palmer, N. Samarth, S. Sangtawesin, D. W. Steuerman, *Science* **2021**, *372*, eabb2823.
[34] G. Burkard, T. D. Ladd, A. Pan, J. M. Nichol, J. R. Petta, *Rev. Mod. Phys.* **2023**, *95*, 025003.
[35] C. Nayak, S. H. Simon, A. Stern, M. Freedman, S. D. Sarma, *Rev. Mod. Phys.* **2008**, *80*, 1083.
[36] J. D. Bommer, H. Zhang, Ö. Gül, B. Nijholt, M. Wimmer, F. N. Rybakov, J. Garaud, D. Rodic, E. Babaev, M. Troyer, D. Car, S. R. Plissard, E. P. A. M. Bakkers, K. Watanabe, T. Taniguchi, L. P. Kouwenhoven, *Phys. Rev. Lett.* **2019**, *122*, 187702.
[37] W. Mayer, M. C. Dartiailh, J. Yuan, K. S. Wickramasinghe, E. Rossi, J. Shabani, *Nat. Commun.* **2020**, *11*, 212.
[38] G. Dresselhaus, *Phys. Rev.* **1955**, *100*, 580.
[39] Y. A. Bychkov, E. I. Rashba, *J. Phys. C: Solid State Phys.* **1984**, *17*, 6039.
[40] S. D. Ganichev, L. E. Golub, *Phys. Status Solidi B* **2014**, *251*, 1801.
[41] L. Golub, E. Ivchenko, *Phys. Rev. B* **2004**, *69*, 115333.
[42] R. Ferdous, E. Kawakami, P. Scarlino, M. P. Nowak, D. Ward, D. Savage, M. Lagally, S. Coppersmith, M. Friesen, M. A. Eriksson, L. M. K. Vandersypen, R. Rahman, *npj Quantum Inf.* **2018**, *4*, 1.
[43] R. M. Jock, N. T. Jacobson, P. Harvey-Collard, A. M. Mounce, V. Srinivasa, D. R. Ward, J. Anderson, R. Manginell, J. R. Wendt, M. Rudolph, T. Pluym, J. K. Gamble, A. D. Baczewski, W. M. Witzel, M. S. Carroll, *Nat. Commun.* **2018**, *9*, 1768.
[44] D. K. Wilson, G. Feher, *Phys. Rev.* **1961**, *124*, 1068.
[45] R. Vrijen, E. Yablonovitch, K. Wang, H. W. Jiang, A. Balandin, V. Roychowdhury, T. Mor, D. DiVincenzo, *Phys. Rev. A* **2000**, *62*, 012306.
[46] T. Tanttu, B. Hensen, K. W. Chan, C. H. Yang, W. W. Huang, M. Fogarty, F. Hudson, K. Itoh, D. Culcer, A. Laucht, A. Morello, A. Dzurak, *Phys. Rev. X* **2019**, *9*, 021028.
[47] S. Lee, H. Koike, M. Goto, S. Miwa, Y. Suzuki, N. Yamashita, R. Ohshima, E. Shigematsu, Y. Ando, M. Shiraishi, *Nat. Mater.* **2021**, *20*, 1228.
[48] M. Fuechsle, J. A. Miwa, S. Mahapatra, H. Ryu, S. Lee, O. Warschkow, L. C. L. Hollenberg, G. Klimeck, M. Y. Simmons, *Nat. Nanotechnol.* **2012**, *7*, 242.
[49] Y. He, S. Gorman, D. Keith, L. Kranz, J. Keizer, M. Simmons, *Nature* **2019**, *571*, 371.
[50] T. F. Watson, B. Weber, Y.-L. Hsueh, L. C. L. Hollenberg, R. Rahman, M. Y. Simmons, *Sci. Adv.* **2017**, *3*, e1602811.
[51] Y. Song, S. D. Sarma, *Phys. Rev. B* **2017**, *96*, 115444.
[52] P. Scarlino, E. Kawakami, P. Stano, M. Shafiei, C. Reichl, W. Wegscheider, L. M. K. Vandersypen, *Phys. Rev. Lett.* **2014**, *113*, 256802.
[53] L. C. Camenzind, L. Yu, P. Stano, J. D. Zimmerman, A. C. Gossard, D. Loss, D. M. Zumbühl, *Nat. Commun.* **2018**, *9*, 1.
[54] Y.-L. Hsueh, L. Kranz, D. Keith, S. Monir, Y. Chung, S. K. Gorman, R. Rahman, M. Y. Simmons, *Phys. Rev. Res.* **2023**, *5*, 023043.
[55] S. Shamim, B. Weber, D. W. Thompson, M. Y. Simmons, A. Ghosh, *Nano Lett.* **2016**, *16*, 5779.
[56] D. Keith, Y. Chung, L. Kranz, B. Thorgrimsson, S. K. Gorman, M. Y. Simmons, *Sci. Adv.* **2022**, *8*, eabq0455.
[57] Y. Wang, C.-Y. Chen, G. Klimeck, M. Y. Simmons, R. Rahman, *Sci. Rep.* **2016**, *6*, 1.
[58] W. Witzel, S. D. Sarma, *Phys. Rev. B* **2006**, *74*, 035322.
[59] P. Stano, D. Loss, *Nat. Rev. Phys.* **2022**, *4*, 672.
[60] S. B. Tenberg, S. Asaad, M. T. Mądzik, M. A. I. Johnson, B. Joecker, A. Laucht, F. E. Hudson, K. M. Itoh, A. M. Jakob, B. C. Johnson, D. N. Jamieson, J. C. McCallum, A. S. Dzurak, R. Joynt, A. Morello, *Phys. Rev. B* **2019**, *99*, 205306.
[61] V. N. Ciriano-Tejel, M. A. Fogarty, S. Schaal, L. Hutin, B. Bertrand, L. Ibberson, M. F. Gonzalez-Zalba, J. Li, Y.-M. Niquet, M. Vinet, J. J. L. Morton, *PRX Quantum* **2021**, *2*, 010353.
[62] F. Borjans, D. Zajac, T. Hazard, J. Petta, *Phys. Rev. Appl.* **2019**, *11*, 044063.
[63] M. Koch, J. G. Keizer, P. Pakkiam, D. Keith, M. G. House, E. Peretz, M. Y. Simmons, *Nat. Nanotechnol.* **2019**, *14*, 137.
[64] A. Morello, J. J. Pla, F. A. Zwanenburg, K. W. Chan, K. Y. Tan, H. Huebl, M. Möttönen, C. D. Nugroho, C. Yang, J. A. van Donkelaar, A. D. C. Alves, D. N. Jamieson, C. C. Escott, L. C. L. Hollenberg, R. G. Clark, A. S. Dzurak, *Nature* **2010**, *467*, 687.
[65] L. Kranz, S. K. Gorman, B. Thorgrimsson, Y. He, D. Keith, J. G. Keizer, M. Y. Simmons, *Adv. Mater.* **2020**, *32*, 2003361.
[66] G. Klimeck, S. S. Ahmed, H. Bae, N. Kharche, S. Clark, B. Haley, S. Lee, M. Naumov, H. Ryu, F. Saied, M. Prada, M. Korkusinski, T. B. Boykin, *IEEE Trans. Electron Devices* **2007**, *54*, 2079.
[67] S. Ahmed, N. Kharche, R. Rahman, M. Usman, S. Lee, H. Ryu, H. Bae, S. Clark, B. Haley, M. Naumov, F. Saied, M. Korkusinski, R. Kennel, M. McLennan, T. B. Boykin, G. Klimeck, in *Encyclopedia of Complexity and Systems Science*, Springer, Berlin, Heidelberg **2009**, pp. 5745–5783.
[68] S. J. Hile, L. Fricke, M. G. House, E. Peretz, C. Y. Chen, Y. Wang, M. Broome, S. K. Gorman, J. G. Keizer, R. Rahman, M. Y. Simmons, *Sci. Adv.* **2018**, *4*, eaaq1459.
[69] L. Kranz, S. K. Gorman, B. Thorgrimsson, S. Monir, Y. He, D. Keith, K. Charde, J. G. Keizer, R. Rahman, M. Y. Simmons, *Adv. Mater.* **2023**, *35*, 2201625.
[70] D. Chadi, *Phys. Rev. B* **1977**, *16*, 790.